JAAS

ROYAL SOCIETY OF CHEMISTRY

PAPER

View Article Online
View Journal | View Issue

Cite this: J. Anal. At. Spectrom., 2026, 41, 438

Determination of elemental concentrations in underwater LIBS plasmas using spectral simulation for copper–zinc alloys

Marion Henkel, *[a] Michelle Siemens,[b] Benjamin Emde,[b] Jörg Hermsdorf[b] and Diego Gonzalez[a]

The analysis of double-pulse LIBS plasmas is a promising technique for environmental neutral underwater material exploration. Since the required spectral analysis methods or suitable calibration curves have barely been investigated for deep-sea applications, a method for spectral simulation and evaluation was developed, enabling evaluation of the elemental concentrations even under non-atmospheric conditions. For this, a method for spectral simulation and evaluation was created, containing the simulation of spectra resulting from multi-elemental plasmas, calculation of data sets with spectral characteristics for various plasma pressures, temperatures and elemental concentrations and the estimation of the plasma parameters and the elemental concentrations related to the measured spectra. Then the accuracy was examined depending on different external parameters, such as laser pulse energy and water pressure. Finally, it was shown that a calibration curve routine for copper–zinc alloys could be created with a mean deviation of 3 at% independent of the laser setup. Furthermore, it was shown that this method for spectral simulation and evaluation is suitable to evaluate LIBS spectra for up to 60 MPa hydrostatic water pressure.

Received 7th July 2025
Accepted 11th November 2025

DOI: 10.1039/d5ja00260e

rsc.li/jaas

1 Introduction

The global demand for critical minerals is experiencing a significant and sustained increase, which is primarily driven by the transition to clean energy and transport technologies. Deep sea mining of manganese nodules appears as a big supply alternative, since the mineral content is potentially higher than the nowadays known mineable land deposits. However, to ensure minimal environmental impact during exploration, a non-invasive method for analyzing elemental composition in deep-sea environments is essential. Underwater, many conventional material analysis techniques are impractical. For instance, on-site mechanical preparation of samples, which is necessary for techniques like mass spectrometry, cannot be conducted. Additionally, creating a stable plasma using an inductively coupled plasma method and applying optical emission or mass spectrometry (ICP-OES/MS) is not currently feasible in water under high pressure. Extracting samples for subsequent analysis under atmospheric conditions is both invasive and costly in terms of time and resources. Therefore, there is a need for a method that avoids the need for sample preparation and does not require direct contact between the measuring device and the sample.

Laser-induced breakdown spectroscopy (LIBS) is an established method for analyzing material samples to determine their elemental concentrations. For this, a pulsed laser beam is focused on the sample surface. There, pulse energies of several tens of millijoules and a pulse duration in the order of nanoseconds are sufficient to evaporate a small amount of the sample material, to produce a plasma and to excite it. Thereafter, the generated plasma radiates specific line intensities during the cool down, which depend on the elemental concentrations.

Previous publications (*e.g.* ref. 1 and 2) have shown that double-pulse LIBS is a promising technique for underwater applications. There, the first laser pulse creates a cavity close to the sample surface. The second laser pulse excites this gaseous state and forms the plasma plume inside the cavity, whose emission provides information about its elemental concentrations. Often, spatial and temporal integrated optical emission spectroscopy (OES) is used to examine the resulting plasma radiation (*e.g.* ref. 3). In industrial applications, line intensities are determined to obtain information about the occurrence of individual elements and their quantities. For this, in industrial applications LIBS is usually operated with calibration curves, which require constant conditions in the generated plasma. These have been well studied and proven for use under atmospheric conditions. However, spectra in underwater LIBS are strongly influenced by external conditions and have considerable pulse-to-pulse fluctuations. Li *et al.*[4] showed a method in

[a]Leibniz Institute for Plasma Science and Technology (INP), Felix-Hausdorff-Straße 2, 17489 Greifswald, Germany. E-mail: marion.henkel@inp-greifswald.de
[b]Laser Zentrum Hannover e.V. (LZH), Hollerithallee 8, 30419 Hannover, Germany

which this fluctuation can be compensated by a combination of spectral measurement and optical imaging of the plasma, resulting in a reduction of the evaluation error to up to 4.07%. The method from Xue *et al.*[5] goes a step further, where measurements were carried out underwater at elevated pressures of up to 50 MPa. For the evaluation, a correction method rooted in functional data analysis was used, which allows the measured spectra at any water pressure to be converted into mappings at shallow water pressure. However, these methods are designed for fixed settings. Evaluation with variable laser parameters for spectral optimization under high water pressures is not provided and will therefore be examined below.

In underwater applications the growth of the plasma plume is limited by the almost incompressible water, which leads to a shorter lifetime and smaller plume size[2] compared to LIBS measurements under atmospheric conditions. This effect is further amplified with increasing water pressure, leading to an increase in the internal cavity pressure, which in turn influences the plasma and thus the measured spectrum.[6] However, most studies for underwater LIBS are limited to shallow water conditions. Tian *et al.*[7] investigated the influence of geometric effects of laser focusing on the generated plasma and Li *et al.*[8] investigated the influence of the laser pulse energy on the spectral line intensity. While no line broadening could be observed in these, because the line width is dominated by the apparatus profile of the detector, the plasma driven line broadening (*e.g.* Stark broadening) becomes more and more relevant with increasing water pressure.[1] The results in ref. 9 indicated such an increase in electron density and temperature with increasing water pressure. Once the water pressure, and thus the pressure in the generated plasma, becomes high enough, the broadening can reach a level where strongly broadened lines overlap, to the point where individual lines can no longer be recognized or they merge into a continuum-like signal. Previous studies have shown (*e.g.* ref. 10) that spectra with separated lines are possible for water pressures up to 40 MPa. Furthermore, Angel *et al.*[11] showed that calibration curves for water pressures up to 28 MPa are reliable for some elements. However, it was also pointed out that the accuracy decreases significantly with increasing water pressure.

For higher external water and internal cavity pressure, the pressure inside the plasma cannot be neglected anymore and previous studies have shown a strong increase in the plasma density[2] and in the continuum radiation and a significant broadening of the atomic emission lines as well as absorption effects at higher hydrostatic pressures[1] up to 60 MPa. Since the plasma pressure and electron temperature have an influence on the plasma composition, *i.e.* the amount of electrons, atoms and ions (see the Saha equation in eqn (3) and (4)), properties in the measured spectrum also change for different laser setups and under external water conditions. Accordingly, there is currently no reliable method to determine the elemental composition of *in situ* samples at water pressures of up to 60 MPa. Therefore, to develop a method for the calculation of plasma compositions, which is independent of external parameters, *i.e.* hydrostatic pressure or laser pulse energy is highly desirable.

In this paper we present a newly developed routine for spectral simulation for the analysis of multi-element spectra to assist underwater LIBS diagnostics. The presented code, which allows the calculation of spectra for different plasma parameters and elemental concentrations during underwater LIBS is, to the best of our knowledge, the first of its kind. Using these spectra, a data set of line intensities and widths could be created. Comparing the spectral characteristics of the data set and those determined from the measured spectra, the elemental concentrations can be obtained. Although the code was first developed for copper–zinc plasma, it can be modified to consider other elements. Furthermore, this method is not limited to the demonstrated LIBS plasma, but can be used for various plasma types and is particularly suitable for applications where variable conditions occur.

The paper is organized as follows: the experimental setup and parameters are given in Section 2. The developed method for spectral simulation and evaluation is explained in Section 3. The results, including calculated elemental concentrations and plasma parameters are shown in Section 4. Section 5 gives a summary and an outlook.

2 Experimental setup

The experimental setup for underwater LIBS consists of a double-pulse laser, a water-filled pressure chamber and a compact spectrometer and is based on the setup previously used in ref. 12 and 13. The schematic experimental setup is shown in Fig. 1.

Two 1064 nm Nd:YAG lasers and pulse energies of up to 160 mJ with a duration of 5 ns to 7 ns were used. The superimposed beams were expanded with a 3× magnification beam expander to a diameter of 18 mm and focused with a 50 mm lens onto the sample surface, which is located in a water-filled pressure chamber. While the first pulse produces a cavity on the sample surface, the second pulse generates a plasma inside the cavity by exciting the vaporized material. The resulting plasma was observed through a sapphire window using a dichroic deflection mirror.

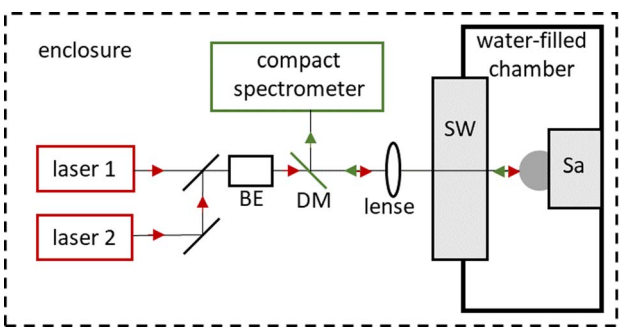

Fig. 1 Sketch of the experimental setup for observation of underwater LIBS plasmas in top view – two Nd:YAG lasers 1064 nm, each up to 160 mJ, 5–7 ns – BE: beam expander – SW: sapphire window – Sa: sample – detection with an compact spectrometer in the coaxial direction using a dichroic deflection mirror (DM). Previously used in ref. 12 and 13.

For this, a trigger scheme, as shown in Fig. 2, was used and the laser pulse energies or the hydrostatic pressure were varied. A short pulse delay t_L of 0.5 μs or 10 μs was successfully tested in ref. 12 with low laser pulse energies and water pressures up to 60 MPa and will therefore be used in the following section.

The plasma plume was observed using a fiber-based compact spectrometer (Avantes AvaSpec ULS17502F-USB2), which is the most expected kind of spectrometer to be used later in industrial deep-sea applications. In this case, an exposure time of 1 ms means that the signal will be integrated over the whole plasma lifetime, skipping the trigger preceding signal at the beginning of the plasma. The absolute calibration of the spectral signal was performed using a tungsten strip lamp (OSRAM Wi 17/G).

As shown in Fig. 3, well resolved lines can be observed from the plasma plume generated underwater. Because of their characteristic spectra, which are well suited for analysis of plasma parameters, copper based samples with varying amounts of zinc have been used in this work. As shown in Fig. 3, an observable change in the spectrum (*e.g.* noise level or line width) could be found, especially for low laser pulse energies, which is caused by the different cavity expansions and material ablations under different laser conditions. This effect can often be observed in plasmas where the external conditions (such as the cavity) also vary, as in this case due to changing laser pulse energy or water pressure. In such cases, constant conditions, as often prevailing in industrial LIBS applications for material analysis, can no longer be assumed, which makes it more difficult to evaluate the spectra.

However, previous time-resolved measurements with a Czerny-Turner spectrometer[16] have shown that the integrated signal is dominated by radiation emitted during the first few hundred nanoseconds of the detection time. Measurements with a time resolution of 100 ns showed an almost flat temperature and pressure profile at a fixed time due to the limited cavity size. A decrease over time could be observed, but the signal is dominated by the signal of the first hundred nanoseconds after the trigger, since the temperature drop is accompanied by a signal drop. Therefore, the plasma can be reasonably approximated as homogeneous for the purposes of these studies.

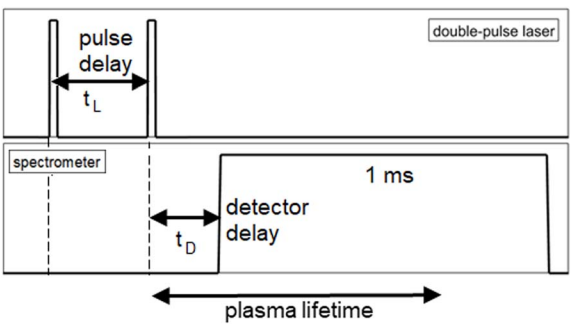

Fig. 2 Sketch of the trigger sequence – two laser pulses, each 5–7 ns duration. Delay t_L between both laser pulses of 0.5 μs or 10 μs, and a delay of t_D = 400 ns between the second laser pulse and the spectrometer to skip the continuum dominated radiation. The used compact spectrometer had an exposure time of 1 ms.

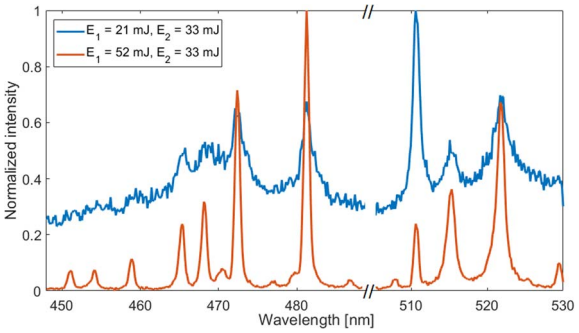

Fig. 3 Spectra of a copper–zinc alloy with 40 at% (DIN EN 12449 CW617N) with two different energies of the first laser pulse E_1 with a pulse delay t_L = 10 μs, measured with a compact spectrometer in the coaxial direction. The measurements were done underwater at 0.1 MPa hydrostatic pressure.

3 Method for spectral simulation and evaluation

In this section the simulation code for a multi-element plasma is described. It is expected that the plasma in this calculation is dominated by atomic and ionic line radiation of the evaporated species. Although the code can be applied to any element with appropriate knowledge of the atomic data, copper–zinc alloys are examined in this paper. The calculations of the spectra shown in the following section were limited to the wavelength range from 452 nm to 537 nm, which takes into account all lines, which could be measured with the experimental setup.

In order to obtain information about the plasma (*e.g.* electron temperature) or of the material to be examined (*e.g.* elemental concentrations) from the measured spectra, a method for spectral simulation and evaluation and various data sets were developed. Using this method, the measurements could be evaluated and compared and various parameters, such as the elemental concentrations, were determined.

The entire method for spectral simulation and evaluation and databases is shown in Fig. 4 and is described below. In this method a local thermal equilibrium (LTE) and a spatially and temporally homogeneous plasma are assumed as a first approximation.

3.1 Single-element plasma composition module

In this module, the partition function and the plasma composition or elemental concentrations are determined for individual elements. Herein, the electron temperature and the plasma pressure are varied and the resulting densities for electrons and neutral/ionized particles are calculated assuming a local thermodynamic equilibrium (LTE). For this purpose, the atomic data for the relevant transitions of the involved elements (here copper and zinc) were taken from the atomic databases from the NIST[17] and Kurucz/Bell.[18]

The partition function Z according to the Planck–Larkin relation,[19] as an element specific weighting factor, depends on the ionization energy E_i of the respective element and the electron temperature T_e of the plasma. All possible transitions

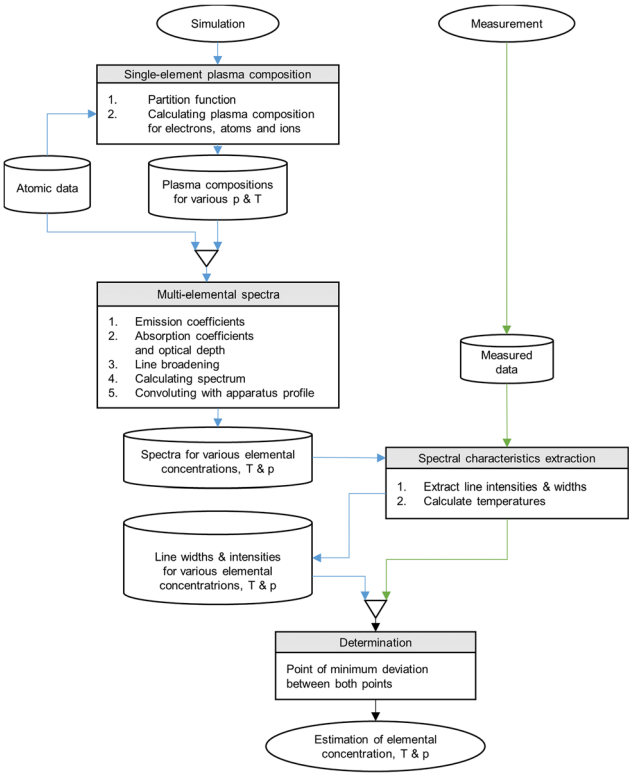

Fig. 4 Flowchart of the modules and data sets of the code package created for the simulation of spectra and the evaluation of measured spectra. Required running time: one-time preparation of data set, few hours and repetitive on-side evaluation, each <1 minute.

of the element are summed up using the respective upper level energy E_k and the respective statistical weights g_k:

$$Z(T) = \sum_k g_k \cdot \exp\left(-\frac{e_0 E_k}{k_B T_e}\right) \quad \text{effects of scattering}$$
$$+ g_k \cdot \exp\left(-\frac{e_0 E_i}{k_B T_e}\right) \cdot \left(\frac{e_0 (E_k - E_i)}{k_B T_e} - 1\right) \quad \text{effects of thermodynamic potential} \tag{1}$$

In the next step, the particle density of the ions n_i depending on the density of the previous ionization level n_{i-1} can be calculated by solving the Saha equation for each species, which are described in more detail in ref. 20–22. The required thermal wavelength of the electrons can be calculated using the de-Broglie wavelength:

$$\lambda_{\text{de-Broglie}} = \sqrt{\frac{h^2}{2\pi m_e k_B T_e}} \tag{2}$$

For a plasma with low ionization levels, the particle densities (e electrons, i ions, n neutrals and t all particles) can be calculated using:

$$\frac{n_e n_i}{n_n} = \frac{Z_e Z_i}{Z_n} \frac{1}{\lambda_{\text{de-Broglie}}^3} \exp\left(-\frac{e_0 E_i}{k_B T_e}\right) \tag{3}$$

where the partition function of the electrons is $Z_e = 2$ and the total particle density $n_t = n_n + n_i$ is given by the plasma pressure ($n_t \sim p/T$).

Since for the relevant temperature range (5000 to 20 000 K) higher ionization is negligible, it can be approximated that $n_e = n_i = \alpha n_t$ and thus $\alpha = n_i/(n_n + n_i)$ as the degree of ionization. Summing the right side of eqn (3) as c_{Saha}, the Saha equation can be solved as follows:

$$\frac{\alpha^2}{1-\alpha} n_t = c_{\text{Saha}}$$
$$n_i = \alpha n_t = -c_{\text{Saha}} \Big/ 2 + \sqrt{(c_{\text{Saha}}^2/4 + c_{\text{Saha}} n_t)} \tag{4}$$

The resulting non-ionized particle and electron density for several elements at 1 bar are shown in Fig. 5. This calculation can now be repeated for different plasma pressures. The determined plasma compositions are then stored in a matrix-shaped data set that contains a variation of the electron temperature and pressure for each element and will be used by the next module for multi-element spectra.

3.2 Multi-elemental spectral module

In this module, the data from the single-element calculations are used and a spectrum for a plasma made of two elements is calculated.

In order to do that, the plasma compositions of electrons and atoms/ions of both elements are calculated using the single-element plasma composition code module, which is based on the Saha equations. Thereby, the electrons are fed by the ionization of both elements and, conversely, as follows, also influence the line broadening of both elements.

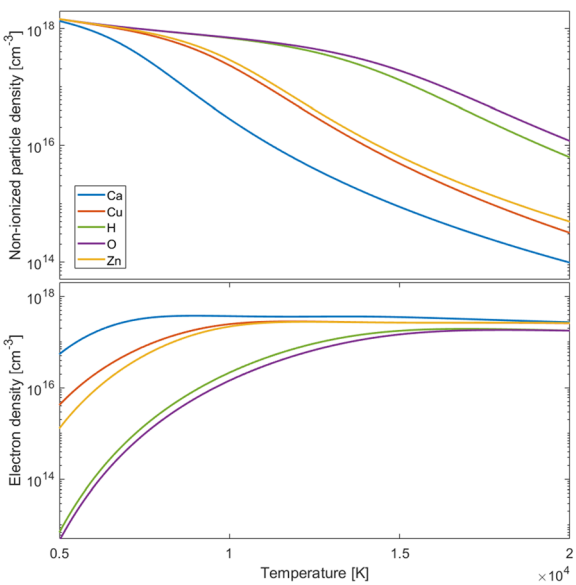

Fig. 5 Top: non-ionized particle density of different elements. Bottom: electron density of the respective elements. All depend on the electron temperature.

In a first approximation it is assumed for the elemental concentration a_k that:

$$n_e = \sum_k a_k n_{e,k} \text{ with } 100\% = \sum_k a_k$$

From here on, a spatial profile for the temperature and particle density should be used for laboratory plasmas. Regardless of how it was generated, many plasmas have the highest temperatures in the core and a decaying temperature profile towards the outside. Although the temperature distribution of the LIBS plasma is not always known, previous experiments at elevated water pressure showed an almost flat temperature profile.[12,13] Accordingly, an approximation of the module considering a homogeneous plasma with a diameter d_p is sufficient. Nevertheless the implemented code can be enhanced to support the spatially solved spectral simulation as well and is therefore able to be applied for other kinds of plasmas.

In order to calculate the spectra, the line widths $\Delta\lambda$ (FWHM) of all involved transitions in the wavelength range are calculated. A detailed description of line broadening mechanisms and shifts of spectral lines in plasmas can be found in ref. 14 and 15. The dominant line broadening effects in the LIBS application using atomic spectral lines are the Stark broadening (Stk), caused by ion-electron collisions, and the van der Waals broadening (vdW), caused by ion–ion collisions and the apparatus profile of the detector. The associated broadening constants C_4 and C_6 can be found in the literature (*e.g.* ref. 23 and 24). Since a difference in a factor of up to 2 between reported values by different researchers can be found, the mean value of these factors is usually taken for this calculation. Furthermore, the mean thermal velocities v of a Maxwell–Boltzmann velocity distribution and the particle densities n of the electrons (e) and atoms/ions (i) will be calculated from the data given from the single-element module:

$$\begin{aligned}\Delta\lambda_{Stk} &= 11.37\frac{{\lambda_k}^2}{2\pi c_0}{v_e}^{1/3}{c_4}^{2/3}n_e\\ \Delta\lambda_{vdW} &= 4.11\frac{{\lambda_k}^2}{2\pi c_0}{v_i}^{3/3}{c_6}^{2/5}n_i\end{aligned} \quad (5)$$

At this point, an additional broadening mechanism should also be mentioned, which is part of the so-called matrix effect. In multi-component plasmas, van der Waals line broadening occurs not only through collisions between heavy particles of the same species, but also between heavy particles of different species. However, there are hardly any reported values for such broadening constants in the literature, so it will not be considered in the following sections.

In addition, the Stark shift is taken into account. The relative shift η of the used copper and zinc lines in the calculated wavelength boundaries was studied by several groups and can be found in the literature (*e.g.* ref. 26):

$$\Delta\lambda_{shift} = \eta_{Stk}\Delta\lambda_{Stk}/2$$

Since van der Waals broadening is only relevant at very low temperatures, and reliable C_6 coefficients in the wavelength range between 452 nm and 537 nm are rare for some transitions, the data shown below will be calculated with purely Stark broadening, convolved with the apparatus profile. Under the observed plasma conditions, this is suitable for comparison with the experimental spectra. However, this does not apply to all types of plasmas, so other types of broadening may need to be considered in other applications.

In the next step, the emission and absorption coefficients for a plasma in LTE are calculated. While the associated radiation transfer equations can be found in ref. 20 in more detail, the most important formulae are summarized as follows.

The emission coefficients ε of the atomic and, if needed, the ionic lines were calculated using the transition probability A_{ul} between upper and lower energy levels, the emitted wavelength λ and the particle density at the upper energy level n_u, which depends on the electron temperature T and the total particle density of the corresponding species n:

$$\begin{aligned}\varepsilon_k &= \frac{c_0 h}{4\pi\lambda_k}A_{ul,k}n_{u,k}\\ n_{u,k} &= \frac{g_{u,k}n_k}{Z_k}\exp\left(-\frac{e_0 E_{u,k}}{k_B T_e}\right)\end{aligned} \quad (6)$$

Furthermore, the dependence of the absorption coefficient κ on the emission coefficient (*e.g.* ref. 25) can be used and the absorption coefficient can be determined for each individual line in the spectrum:

$$\kappa_k = \frac{2/\pi}{\Delta\lambda_{Stk/vdW}}\frac{\varepsilon_k}{\text{Planck}(\lambda_k, T_e)} \quad (7)$$

Finally, the spectrum can be calculated by integrating over the line of sight using the emission and absorption coefficients of all involved transitions or lines and solving the differential radiation transport calculation:

$$dL(x) = (\varepsilon(x) - \kappa(x)L(x))dx \quad (8)$$

Because the plasma is assumed to be homogeneous in temperature and density/pressure in this method, the emission and absorption coefficients in the numerical solution are constant. Therefore the solution of the radiation transport equation can be solved, approaching a homogeneous plasma with a diameter d_p:

$$\begin{aligned}L(p, T_e) &= \text{Planck}(\lambda_k, T_e)\left(1 - \exp\left(-\sum_k \tau_k\right)\right)\\ \tau_k &= \kappa_k d_p\end{aligned} \quad (9)$$

where τ is the so-called optical depth, which is an indicator of the total absorption in the plasma. Two exemplary simulated spectra for copper–zinc alloys with different amounts of zinc are shown in Fig. 6.

This calculation can now be repeated for different plasma pressures, electron temperatures and elemental concentrations.

The resulting spectra are stored in a data set and will be used by the next module for comparison of selected parameters with the measured spectra.

3.3 Spectral characteristic extraction module

In order to extract spectral characteristics such as line widths and intensities, an evaluation routine was implemented. This module can be applied to both the simulated spectra and the measured ones.

In the shown cases, a Lorentz profile of the lines was used to simplify the calculation, since Stark broadening is dominant in underwater applications. However, in this module Gaussian or Lorentz profiles can also be taken into account if the apparatus profiles or van der Waals broadening are dominant.

For further evaluation, the full width at half maximum (FWHM) line width and the integrated line intensity (L) of each line in the observed wavelength range can be extracted using a fit function for Lorentz profiles. These values were then saved for the calculation of various plasma parameters, as described in the following section:

(1) Electron temperature: the temperature will be calculated using the Boltzmann plot method by exploiting the atomic line integrals of one of the elements. In the data shown in Section 4.2, copper is most suitable due to the different energy levels of the detected lines within the observed spectral range.

(2) Total particle density: the radiation of a specific atomic line is defined by the neutral or ionized particle density at the respective upper energy level, which depends on the electron temperature and total particle density of the respective element. In the shown data the lines at 481.1 nm for zinc and 521.8 nm for copper were used. Often, instead of particle density, plasma pressure ($p \sim nT$) is used as a value here.

(3) Electron density: the atomic lines can be broadened by several effects. However, lines in the shown data are dominantly Stark-broadened. This depends on the electron density and temperature. Using the line width of the copper related line at 521.8 nm, the total electron density can be calculated which is defined by the sum of the partial electron densities of all occurring elements.

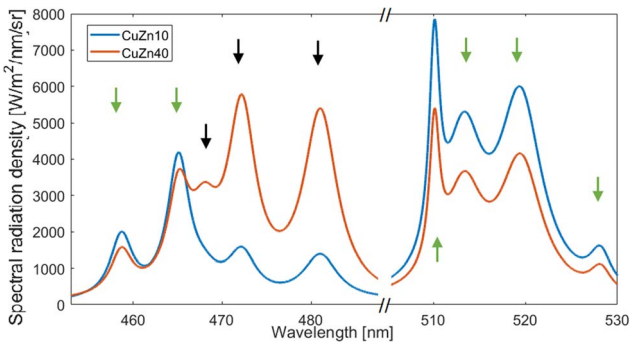

Fig. 6 Simulated spectra of copper–zinc alloys for 10 at% and 40 at% amounts of zinc. Green arrows: lines related to copper and black arrows: lines related to zinc. Input parameters: plasma pressure of 10 bar and electron temperature of 18 000 K.

(4) Elemental concentrations: the line integral of a strong line of each element, here 521.8 nm for copper and 481.1 nm for zinc, can be used to calculate the elemental concentrations. Since the line integral of an atomic line depends on various parameters (*e.g.* temperature, density, and optical thickness), a direct reverse calculation from the line integrated intensity or the ratio between two lines of different elements is not possible. Therefore, the comparison with a data set is the most promising method, using the calculated temperature and extracted line intensities as input parameters. The method will be described in the following section.

3.4 Determination module

Since the line intensities of different lines depend not only on the elemental concentrations, but also on the plasma parameters, a direct reverse calculation from the fitted data with a reasonable computational effort is not possible. Although it is possible to derive temperatures and sometimes even electron densities directly from the spectrum, as described above, the line intensities are particularly dependent on the atomic and ionized particle densities, which cannot be determined directly but have to be laboriously calculated. Therefore, the desired values, such as elemental concentrations or plasma pressure, are determined from a comparison with the fitted values of the line integrals and if necessary the line widths of simulated spectra and the point of minimum deviation between both inputs, measured and simulated spectra.

First, the spectra for given temperatures, plasma pressures and elemental concentrations were calculated and the spectral characteristics (line widths and intensities) were extracted and stored in a matrix-shaped data set. Second, the spectral characteristics are calculated from the measured spectra too and compared with the corresponding data set. The most suitable parameters for the LIBS spectra of the copper–zinc alloys shown below are the line width of the copper related line at 521.8 nm due to the dominant Stark broadening and the zinc related line at 481.1 nm, due to the high intensity of both lines.

However, it was found in previous experiments[12] that an additional strong electron contributor, most probably hydrogen and oxygen from water, exists in underwater LIBS measurements. While their line intensities in the observed wavelength range are negligible compared to the lines related to copper even at high partial pressures, the additional electron density can exceed the electron density of a pure copper plasma by several orders of magnitude, as shown in ref. 12. For this reason, the line width, as an indicator of the electron density, is not used as an input parameter for the determination of the elemental concentration in the shown calculations. Although the evaluation routine delivers acceptable results with relatively calibrated lines (or more precisely line ratios) using line widths as an additional input parameter, absolutely calibrated spectra should be used in this case in order to have line intensities for the determination of the plasma parameters. While relative calibration only corrects for the wavelength-dependent sensitivity of the optical components and detectors, absolute calibration additionally converts the measured signal into physical

units, usually a spectral radiation density. This value depends not only on the temperature but also on the particle density of the species involved, which react with different sensitivities to plasma pressure and electron temperature due to the different ionization energies and energy levels (see Section 3.1).

First, the electron temperature T_e has to be calculated by using the Boltzmann plot method. This method is usually applied to optically thin plasmas where the self-absorption is negligible. Even if the observed plasma density in the measured spectra is quite high, the element-specific density (here copper or zinc) is small enough to fullfil the assumption. Second, the deviation of the line intensities (or widths) x from the measured data m from each data point k of the existing data set d is calculated to find the point of minimum deviation δ_i and to determine the partial plasma pressures p_k and elemental concentrations a_k:

$$\delta_i = \frac{(x_d(T_e) - x_m)^2}{{x_m}^2} \min\left(\sum \delta_i\right) \rightarrow p_k, a_k \qquad (10)$$

4 Results and discussion

4.1 Analysis of spectral characteristic dependence on plasma parameters

Using the code modules described in Sections 3.1 and 3.2, a data set for copper–zinc alloy samples was calculated for known values of plasma pressure, electron temperature and elemental concentrations and tested with measured spectra. However, it should be noted that the plasma pressure cannot be obtained directly from the measured spectrum, even though it does affect the spectral lines. Instead, the plasma pressure is determined indirectly from quantities that can be extracted from the spectrum: the metal vapor density using line intensities, the electron density using line widths, and the electron temperature using line ratios. In the method applied here, this step is bypassed, since the measured spectra are compared directly with a data set in which the plasma pressure, resulting from the combination of density and temperature, is already included as a parameter.

However, it must be mentioned that the plasma pressure cannot be derived directly from the spectrum, even though it does of course have an influence on the measured spectrum. Rather, the plasma pressure is determined using the dependence on the previously mentioned parameters. In order to do that, the atomic line intensities at 481.1 nm for zinc and 521.8 nm for copper, the line width of the copper related atomic line and the ratio between both lines were used.

Although the determination of the plasma composition and its elemental concentrations is independent of the laser setup, the data set containing the information from the simulated spectra is limited to the respective diagnostic setup due to effects from apparatus profiles and therefore must be calculated individually for each spectrometer. In this case, the evaluations were focused on the atomic lines of copper and zinc in the wavelength range of 452 nm to 537 nm, as the transitions of the respective ions are significantly weaker. The simulated line integrated intensity at 521.8 nm for a pure copper sample of the resulting data set can be seen in Fig. 7. Moreover, the measured intensities can be used to find the plasma pressure using the electron temperature determined by using the Boltzmann plot method. In such a way, plasmas can even be reliably distinguished from measurements with similar line widths but different magnitudes of plasma pressure (see blue crosses in Fig. 7).

In order to compare the measured spectra with the data set, information about the electron temperature (*e.g. via* the Boltzmann plot method) or the elemental concentrations must be available. The other two parameters (plasma pressure, electron temperature or elemental concentrations) are then obtained using the determination module. If the elemental concentrations are unknown and need to be determined, the temperature has to be calculated first. Then, the estimation module is used to find the plasma pressure and the elemental concentrations. For this calculation, the different behaviors or the different dependencies of the line integrated intensity and the ratio between lines of both species on parameters are exploited, as shown in Fig. 8.

It can be seen that the ratio of two lines of different elements, here copper and zinc, depends not only on the elemental concentrations, but also slightly on the plasma pressure. The deviation of the determined zinc concentration over the whole range of plasma pressure for a specific line ratio is negligible for small atomic proportions. However, it makes a significant difference for a larger amount of zinc. As a result, while evaluating small proportions is possible with sufficient accuracy using relatively calibrated spectra, absolute calibration is necessary for reliable evaluation of samples with higher proportions. In this case, the plasma pressure can be determined using the absolute values of a line integral, or to be precise, the amount of zinc and the plasma pressure can be determined using the point of minimum deviation from the data set.

However, it is striking that the line width, which in the measurements is dominated by Stark broadening, is significantly larger than would be expected from the determined metal

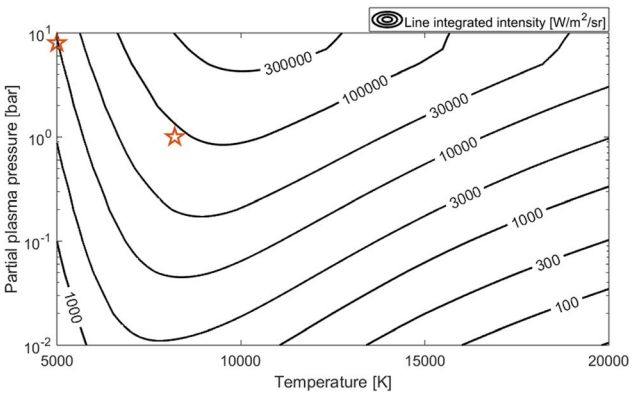

Fig. 7 Isoline plot of the line integrated intensity at 521.8 nm from the created data set depending on electron temperature and plasma pressure for pure copper. Orange stars: both data points have a similar line width of 1 nm.

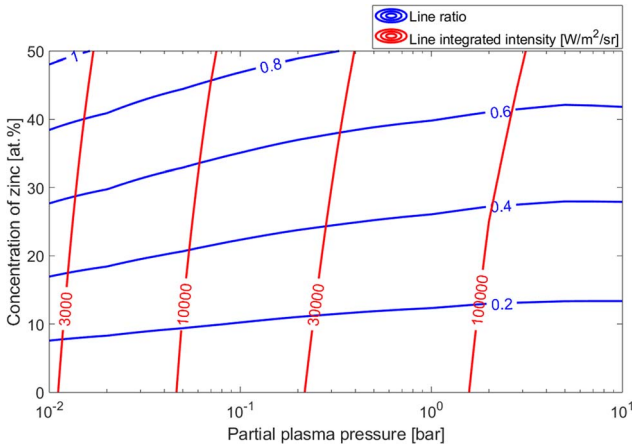

Fig. 8 Isoline plots of the line integrated intensity at 521.8 nm (red) and the line integrated intensity ratio of the 481.1 nm line to the 521.8 nm line (blue), both from the created data set depending on the plasma pressure and the concentration of zinc for 8000 K.

vapor density. Since this type of broadening depends on the electron density, this indicates the presence of additional electron sources. That's why it is assumed from the measured spectra that underwater LIBS plasmas contain a fairly high proportion of hydrogen and oxygen, which also contribute to the electron density, although their line intensities in the observed wavelength range are several orders of magnitude smaller than the copper line intensities for a large pressure range. Therefore, it is not plausible to use the Stark broadening to determine the electron density with the obtained data of this experiment.

Finally, the presented method is more complex in preparation compared to other common evaluation methods, such as comparing the deviation of entire spectra according to Pearson.[27] However, it is less susceptible to absorption effects or thermal imbalance, which sometimes only change individual lines. By specifically selecting lines with minimal changes, a comparatively more precise determination is also possible in these cases.

4.2 Investigation of sample compositions

For the test of the shown method as a substitute of calibration curves, as usually used in industrial LIBS applications, various copper–zinc alloys were used. For this, probes with elemental concentrations were used, which are defined by the DIN standard EN 12449.

First, it was tested whether the laser setup has an influence on the accuracy of the evaluation routine. For this purpose, the laser pulse energy of both pulses in the LIBS setup was varied and the measured spectrum for a common copper–zinc alloy with 40 at% (brass/CW612N) was evaluated to determine the concentration of zinc. As shown in Fig. 9, the calculated value only deviates from the declared value by a maximum of 5 at% under shallow water conditions.

Second, several copper–zinc alloys with different concentrations of zinc were used (DIN EN 12449 CW500L to CW509L) to check the feasibility of a calibration curve using the presented method. In order to do that, a pulse delay between both laser pulses of $t_L = 0.5$ µs had to be chosen, because the life time of the cavity and the plasma is significantly reduced at higher water pressures as occurring in deep-sea, as shown by Siemens *et al.*[6] In addition, small laser pulse energies were used since, as previous evaluations have shown, these lead to smaller line broadening in the measured spectrum,[12] which is advantageous for an evaluation. It was found that a linear relationship between the calculated and declared amount of zinc could be shown with a mean deviation of 3 at% (see Fig. 10).

In the last step, it was examined how the elevated hydrostatic pressure in the underwater LIBS setup affects the accuracy of the evaluation. As shown in Fig. 11, the deviation of the calculated value is significantly increased and reaches values of up to 12 at%. The reason for this result is that the plasmas observed at elevated hydrostatic pressure can no longer be assumed as always optically thin, due to the smaller cavity size and thus the higher plasma pressure. Furthermore, effects caused by trace elements (*e.g.* lead in brass alloys) were not taken into account, which in industrial applications are usually described by the so-called matrix effects. Furthermore, the homogeneity of the composition of the sample on the locally examined surface is not known, which can be counteracted by measuring and averaging multiple times at different positions.

Both effects can lead to an increasing error in the evaluation that will be investigated in more detail in the future. Nevertheless, it could be shown that it is possible to determine the elemental concentrations using the proposed method even in the defined parameter ranges despite strongly broadened spectra and a suboptimal signal-to-noise ratio as usually occurs under deep-sea conditions, comparable to shallow water spectra as in Fig. 3.

The results shown here refer exclusively to a two-element plasma of copper and zinc. However, the routine can easily be extended to more elements. Since in the shown simulations, the plasma is always assumed to be in thermodynamic equilibrium, the number of elements examined should not influence the accuracy. However, this is subject to the same limitations as

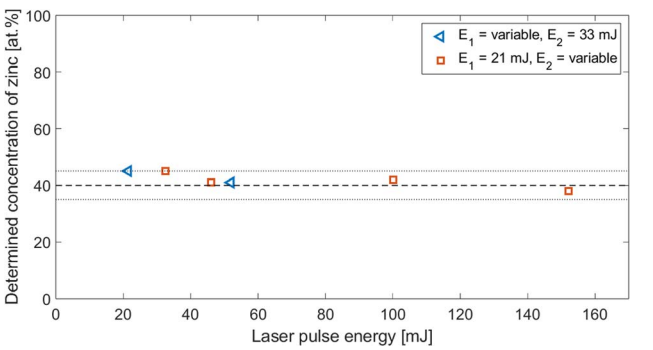

Fig. 9 Determined concentration of zinc depending on the laser pulse energy for a copper–zinc alloy (DIN EN 12449 CW612N) using a pulse delay of $t_L = 10$ µs. Triangles: variation of the first laser pulse energy, squares: variation of the second laser pulse energy, dashed line: declared concentration of zinc, and dotted lines: ±5 at% deviation. All data points are single measurements.

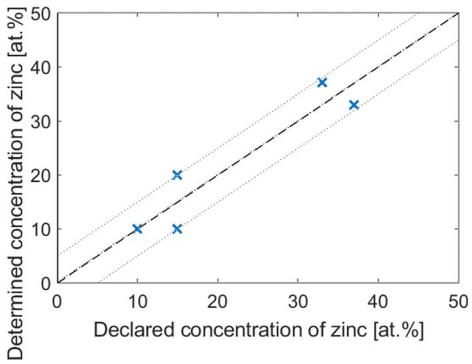

Fig. 10 The determined concentration of zinc plotted against the declared amount of zinc for copper–zinc alloys (DIN EN 12449 CuZn10 to CuZn37). Crosses: calculated values, dashed line: indicates that the determined concentration is equal to the declared concentration of zinc, and dotted lines: ±5 at% deviation with a mean deviation of 3 at%. Laser setup: $E_1 = 21$ mJ, $E_2 = 33$ mJ and a pulse delay of $t_L = 0.5$ µs. All data points are single measurements.

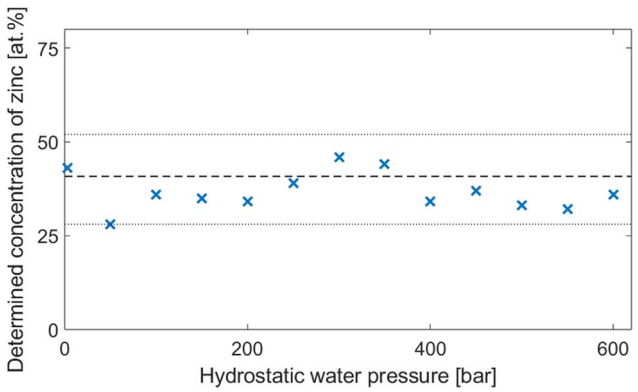

Fig. 11 Determined concentration of zinc depending on the hydrostatic water pressure for a copper–zinc alloy (DIN EN 12449 CW612N). Crosses: determined values, dashed line: declared concentration of zinc, and dotted lines: ±12 at% deviation. Laser setup: $E_1 = 21$ mJ, $E_2 = 33$ mJ and a pulse delay of $t_L = 0.5$ µs. All data points are single measurements.

other evaluation methods (*e.g.*, industrial LIBS). Line intensities that differ by orders of magnitude or overlap of lines from different elements are due to the measurement and not due to the evaluation, so the influence of these measurement-related causes on the accuracy must be investigated more closely in the future.

5 Conclusions

In this manuscript, a code set for evaluation of the elemental concentrations of materials in underwater LIBS was shown. It enables evaluating spectra in various plasma applications. For this purpose, a modular code was created, which includes the calculation of single-element plasma compositions and multi-element spectra, extraction of spectral characteristics of both measured and simulated data and determination of plasma parameters and elemental concentrations.

To test the accuracy of the method, underwater LIBS plasmas were used, which were generated using a double-pulse laser setup focused on the surface of a copper–zinc alloy. Using this method for spectral simulation and evaluation, a data set was calculated including the line width and intensity of the atomic copper line at 521.8 nm and the line ratio to the atomic zinc line at 481.1 nm. It could be shown that it is possible to determine the elemental concentrations and the partial plasma pressures by finding the point of minimum deviation between the data set and the measured values.

In order to prove the accuracy of the method, measurements with different laser pulse energies were conducted. It was shown that the deviation of the determined concentration of zinc regarding the laser pulse energy is below 5 at%. Furthermore, measurements of copper–zinc plasmas with different concentrations of zinc showed that a calibration curve routine with a mean deviation of 3 at% can be achieved. With increasing external pressures, in this case due to the underwater application, the deviation increases. Nevertheless, applicability could be demonstrated for hydrostatic water pressures up to 60 MPa.

It was shown that the created method for spectral simulation and evaluation enables determination of elemental concentrations in plasmas in different parameter ranges. This allows measurements with LIBS systems without having precise data about the laser system or the experimental setup. Creating a data set adapted to a specific spectrometer system enables an on-site evaluation in a reasonable amount of time especially for measurements with varying external conditions.

Conflicts of interest

There is no conflict to declare.

Data availability

The experimental spectra related to the shown results, the used atomic data for simulation and the generated data matrix of line intensities and ratios as shown in this manuscript are openly available at DOI: https://doi.org/10.34711/inptdat.1012.

Acknowledgements

This project was funded by the Deutsche Forschungsgemeinschaft (DFG, German Research Foundation) – project number 454848899. The authors would like to thank Dr Steffen Franke for providing a first version of the computational code including the calculation of single-elemental plasma compositions and single-elemental spectra.

Notes and references

1 B. Emde, *et al.*, Double pulse laser induced breakdown spectroscopy at 600 bar water pressure, *Proced. CIRP*, 2020, **94**, 791–795.
2 V. Lazic and S. Jovićevi, Laser induced breakdown spectroscopy inside liquids: Processes and analytical

aspects, *Spectrochim. Acta B Atom Spectrosc.*, 2014, **101**, 288–311.
3 B. Thornton and T. Ura, Effects of Pressure on the Optical Emmisions Observed from Solids Immersed in Water using a Single Pulse Laser, *Appl. Phys. Express*, 2011, **4**, 022702.
4 Q. Li, *et al.*, Improvement in the analytical performance of underwater LIBS signals by exploiting the plasma image information, *J. Anal. At. Spectrom.*, 2020, **35**, 366–376.
5 B. Xue, *et al.*, Quantification of underwater LIBS at varying ambient pressures towards deep-sea applications, *J. Anal. At. Spectrom.*, 2025, **40**(11), 3138–3149.
6 M. Siemens *et al.*, Investigation of the detection limits of zinc and copper in brass alloys at water pressures of up to 600 bar using double-pulse LIBS, *13th CIRP Conference on Photonic Technologies (LANE)*, 2024.
7 Y. Tian, *et al.*, Laser focusing geometry effects on laser-induced plasma and laser-induced breakdown spectroscopy in bulk water, *J. Anal. At. Spectrom.*, 2019, **34**, 118.
8 W. Li and W. Zhou, Comparative Study of Underwater Single Pulse and Orthogonal Double Pulse Laser-Induced Breakdown Spectroscopy of Barium Element in Solution, *Chin. J. Lasers*, 2019, **46**(9), 911003.
9 H. Hou, *et al.*, Plasma condensation effect induced by ambient pressure in laser-induced breakdown spectroscopy, *Appl. Phys. Express*, 2014, **7**, 032402.
10 A. Matsumoto and T. Sakka, A review of underwater laser-induced breakdown spectroscopy of submerged solids, *Anal. Sci.*, 2021, **37**, 1061–1072.
11 S. M. Angel, *et al.*, Underwater measurements using laser induced breakdown spectroscopy, *J. Anal. At. Spectrom.*, 2016, **31**, 328–336.
12 M. Henkel, *et al.*, Double-pulse LIBS in water with up to 600 bar hydrostatic pressure and up to 150 mJ energy of each pulse, *Spectrochim. Acta B Atom Spectrosc.*, 2023, **213**, 106877.
13 M. Siemens, *et al.*, Investigation of Laser-Induced Cavity and Plasma Formation in Water Using Double-Pulse LIBS, *Physics*, 2024, **6**(1), 108–122.
14 E. Oks *et al.*, *Stark Broadening of Spectral Lines in Plasmas*, MDPI Books, ISBN978-3-03897-455-0, 2018.
15 N. Konjević, Plasma broadening and shifting of non-hydrogenic spectral lines: present status and applications, *Phys. Rep.*, 1999, **316**, 339–401.
16 M. Henkel, *et al.*, Laser-induced plasma formation in water with up to 400 mJ double-pulse LIBS, *Plasma Sci. Technol.*, 2024, **26**, 015506.
17 A. Kramida, Yu. Ralchenko, J. Reader and NIST ASD Team, *NIST Atomic Spectra Database (Version 5.10)*, National Institute of Standards and Technology, Gaithersburg, MD, 2022, https://www.nist.gov/pml/atomic-spectra-database.
18 R. L. Kurucz and B. Bell, *Atomic Line Data*, Smithsonian Astrophysical Observatory, Cambridge, Mass, 1995, https://lweb.cfa.harvard.edu/amp/ampdata/kurucz23/sekur.html.
19 F. J. Rogers, Occupation Numbers for Reacting Plasmas: The Role of the Planck-Larkin Partition Function, *Astrophys. J.*, 1986, **310**, 723.
20 S. Günter, *Einführung in die Plasmaphysik 1*, Max-Planck-Institut für Plasmaphysik, Technische Universität München, 2013.
21 S. Dattagupta, On the Saha Ionization Equation, *Resonance*, 2018, **23**, 41–56.
22 W. Ebeling, Equation of state and saha equation of partially ionized plasmas, *Physica*, 1968, **38**, 378–388.
23 P. Meenakshi Raja Rao, *et al.*, Line broadening studies in low energy plasma focus, *Plasma Phys.*, 1989, **32**, 627–639.
24 M. Born, Line broadening measurements and determination of the contribution of radiation diffusion to thermal conductivity in a high-pressure zinc discharge, *J. Phys. D:Appl. Phys.*, 1999, **32**, 2492.
25 N. Bogatyreva, *et al.*, Mean absorption coefficients of air plasmas, *J. Phys.: Conf. Ser.*, 2011, **275**, 012009.
26 Y. Fujioka and S. Nakamura, Stark Effect for the Spectra of Silver, Copper, and Gold, *Astrophys. J.*, 1927, **65**, 201.
27 S. M. Zaytsev, A. M. Popov and T. A. Labutin, Stationary model of laser-induced plasma: Critical evaluation and applications, *Spectrochim. Acta, Part B*, 2019, **158**, 105632.